Helicene-derived aggregation-induced emission conjugates with highly tunable circularly polarized luminescence

Chengshuo Shen, Fuwei Gan, Guoli Zhang, Yongle Ding, Jinghao Wang, Ruibin Wang, Jeanne Crassous, Huibin Qiu

HAL Id: hal-02531287

https://univ-rennes.hal.science/hal-02531287

Submitted on 12 May 2020

Tunable Circularly Polarized Luminescence of Helicene-Derived Aggregation-Induced Emission Adducts

Chengshuo Shen[1,2], Fuwei Gan[1], Guoli Zhang[1], Yongle Ding[1], Jinghao Wang[1], Ruibin Wang[3], Jeanne Crassous[4], Huibin Qiu[1,2]

[1]School of Chemistry and Chemical Engineering, State Key Laboratory of Metal Matrix Composites, Shanghai Jiao Tong University, Shanghai 200240, China. [2]State Key Laboratory for Modification of Chemical Fibers and Polymer Materials, College of Materials Science and Engineering, Donghua University, Shanghai 201620, China. [3]Instrumental Analysis Center, Shanghai Jiao Tong University, Shanghai 200040, China. [4]Univ Rennes, Institut des Sciences Chimiques de Rennes, UMR CNRS 6226, Campus de Beaulieu, Rennes 35042, France. Correspondence and requests for materials should be addressed to H.Q. (email: hbqiu@sjtu.edu.cn).

Abstract: Chiral organic molecules play an important role in generating circularly polarized luminescence (CPL) with high quantum yield and tunable colors. However, their CPL performance is virtually limited by the small dissymmetric factor $|g_{lum}|$ value and the aggregation-caused quenching issue in the solid state. Here, we report a series of luminescent molecules with tailored marriage of helicenes and aggregation-induced emission (AIE) luminophores. The resulting adducts are highly fluorescent in the aggregated state with color varying from blue to green and quantum yield up to 37.0%, depending on the linkage position, conjugation and length. The efficient association of the helical conjugated skeleton of helicene and the AIE moiety also enables a relatively high $|g_{lum}|$ value ranging from 0.001 to 0.011. Notably the $|g_{lum}|$ value could be further enhanced to ca. 0.015 by the substitution of two AIE luminophores onto a single helicene. This work provides a facile synthetic strategy for advanced molecular CPL materials, and would also favor the fabrication of high-performance circularly polarized organic light-emitting devices.

Circularly polarized light is a type of electromagnetic waves with its electric field vector turning along a helical trajectory, and can be distinguished as right- and left-handed lights according to its handedness.[1] In nature, species such as beetles and shrimps prevalently use circularly polarized light in signaling or covert communication.[2-4] For practical applications, circularly polarized light is also of crucial importance in quantum teleportation,[5] information encryption and storage,[6,7] chemical and biological probing,[8-11] asymmetric photosynthesis,[12,13] and electrooptical devices.[14-16] Recently, circularly polarized luminescence (CPL) materials are emerging as a key portal to generate circularly polarized light and can directly emit circularly polarized light without using a circularly polarized filter.[17] Among all CPL materials, chiral organic molecules[18-20] play an indispensable role prominently as a result of their tunable color, strong intensity, high stability and facile processing characters compared with other materials such as chiral lanthanides[21] and chiral assembly systems.[22,23] However, the practical utilization of CPL-active organic molecules is substantially limited by the low dissymmetric factor $|g_{lum}|$ ($g_{lum} = 2(I_L - I_R)/(I_L + I_R)$, where I_L and I_R are the intensities of left- and right-handed circularly polarized emissions, respectively) and the potential aggregation-caused luminescence quenching in the solid state.

Aggregation-induced emission (AIE) provides an effective way to overcome the aggregation-caused luminescence quenching issue[24,25] and appears to be useful for the construction of new CPL materials. However, most of CPL active AIE materials were achieved via supramolecular, polymer or liquid crystal pathways,[23] which substantially limits the further applications due to the structural instability and the obscure structure-function relationship. Up to date, only a few CPL active AIE small molecules were prepared, majorly by tethering chiral binaphthyl elements onto AIE luminophores.[26,27] Nevertheless, the $|g_{lum}|$ value of these molecular materials were found to be less than 5×10^{-3}, probably as a consequence of the insufficient association between the chiral elements and the AIE luminophores.

Helicenes are constituted of *ortho*-fused spirally arranged aromatic rings, and exhibit prominent chiroptical properties because of the large rotational strength from the inherent electron transitions

along the helical π-conjugated skeleton.[28,29] Compared with other chiral organic molecules, helicene derivatives are of great importance for CPL materials due to their relatively large CPL signals.[19,30-35] Here, we develop a facile pathway to prepare highly luminescent AIE materials with tunable emission color and high $|g_{lum}|$ value by tethering or fusing helicene units as chiral auxiliary onto AIE-active tetraphenylethene (TPE) units. Through flexible marriage of AIE luminophores with ready-made helicenes by click chemistry or metal-catalyzed coupling reactions, a series of AIE-helicene adducts have been synthesized, and they exhibit blue to green emission colors (λ_{em} = 450 ~ 520 nm) in the aggregated state with quantum yield (Φ) of 3.8 ~ 37.0% and $|g_{lum}|$ value up to 0.015. This work provides new opportunities for the design and synthesis of advanced CPL materials, which would be useful for the preparation of high-performance circularly polarized light-emitting devices.

Results

Non-conjugated AIE-helicene adducts

TPE is a typical AIE luminophore and exhibits strong luminescence towards aggregation (Φ = 49.2% in film).[36,37] It was anticipated that by close linking the chirality of helicene can be transferred to the TPE luminophore and thus induce CPL (Fig. 1a). To this end, we first synthesized two adducts, namely **2-TBTH** and **4-TBTH,** by tethering TPE onto 2- and 4-ethynyl[6]helicenes, respectively, through click chemistry (copper-catalyzed azide-alkyne cycloaddition reaction) (Fig. 1b, see Supplementary Methods for synthetic details).
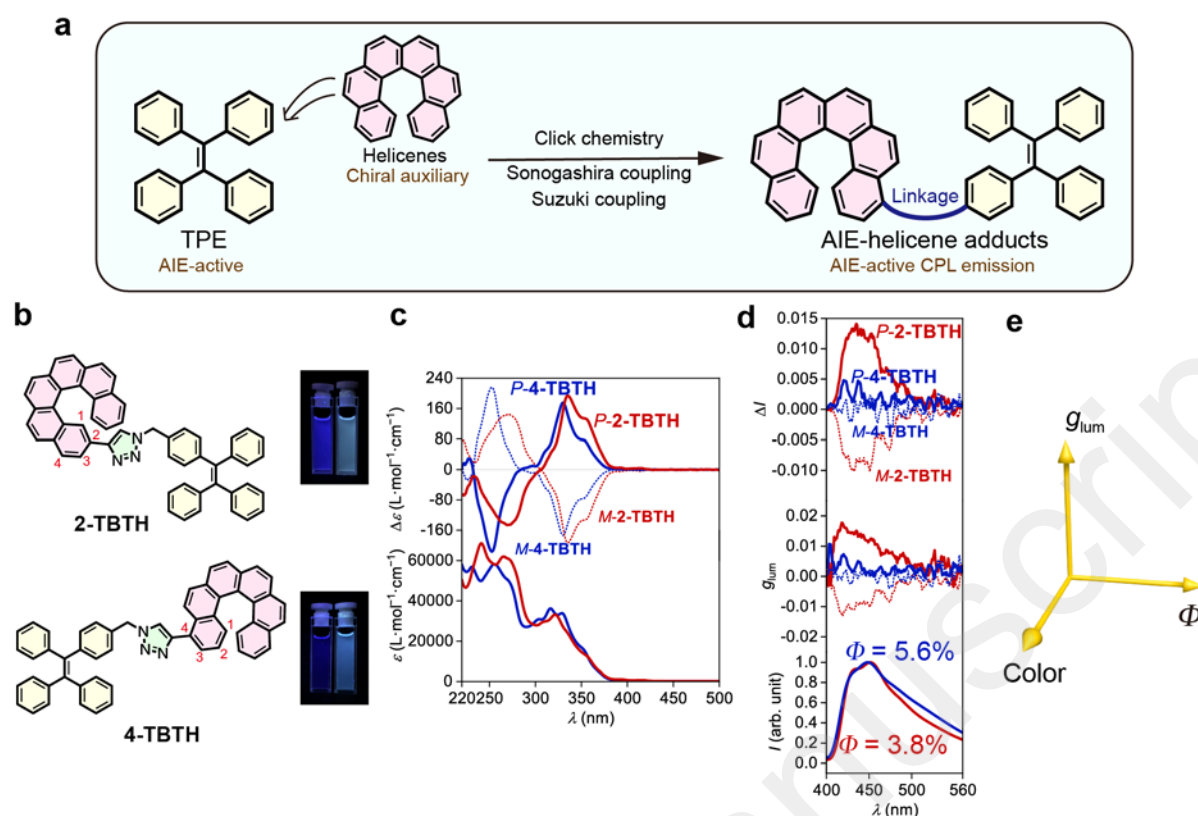
Figure 1 | Design of AIE-helicene adducts and CPL performance of non-conjugated AIE-helicene adducts. (a) Illustrative representation for the synthetic strategy of AIE-helicene adducts via tunable linking of helicenes (as chiral auxiliary) and AIE-active TPE units through click chemistry, Sonogashira coupling and Suzuki coupling reactions. (b) Molecular structures of **2-TBTH** and **4-TBTH**, and corresponding photographs showing their luminescence behavior in THF (left) and a mixture of THF and H_2O (1 : 19, v/v) (right) with a concentration of 2.0×10^{-5} mol·L^{-1} under 365 nm UV light irradiation. (c) UV-vis and ECD spectra of **2-TBTH** and **4-TBTH** in THF with a concentration of 2.0×10^{-5} mol·L^{-1} at 298 K. (e) Luminescence, CPL and g_{lum} spectra of **2-TBTH** and **4-TBTH** in a mixture of THF and H_2O (1 : 19, v/v) with a concentration of 2.0×10^{-5} mol·L^{-1} at 298 K with excitation at 365 nm. (e) Three key factors (g_{lum}, quantum yields Φ, and color) for the evaluation of CPL materials.

As shown in Fig. 1c, both **2-TBTH** and **4-TBTH** showed positive Cotton effects around 335 and 330 nm and negative Cotton effects around 270 and 252 nm for the *P*-enantiomers (mirror image for the *M*-enantiomers), respectively, indicating a characteristic nature of [6]helicene. When investigating the luminescence property (Fig. 1d), to our surprise, these two molecules failed to exhibit typical AIE properties. Along with an increase of the water fraction from 0% to 95%, the

luminescence showed no obverse enhancement (see Supplementary Figs. 44 and 45 for luminescence spectra with different water fractions) and the quantum yields in the aggregated state were only 3.8% and 5.6%, much smaller than TPE itself. This was probably because that the helicene moiety emits both in solution and in the aggregated state, and the relatively loosen aggregation structures might also impair the AIE feature of the TPE domain. Regarding their CPL performance, **2-TBTH** was found to be CPL active and showed relatively high g_{lum} values of +0.012 and −0.010 for the *P*- and *M*-enantiomers (at ca. 450 nm, maximum emission wavelength, $\lambda_{em,max}$), respectively. On the contrary, **4-TBTH** was found to be CPL inactive.

Fully conjugated AIE-helicene adducts

Although the g_{lum} of **2-TBTH** appears to be prominent (presumably majorly derived from the helicene-triazole moiety), its quantum yield is extremely low and the emission color is limited in the blue region. In principle, an ideal CPL material system should be characterized by a high $|g_{lum}|$ value, a high quantum yield and a large diversity in emitting color (Fig. 1d). To this end, we further prepared **2-TPEH** and **4-TPEH** (Fig. 2a left, see Supplementary methods for synthetic details) by linking helicene and TPE through a conjugated alkynyl bridge.[38,39]

In the absorption spectra (Fig. 2b left), both **2-TPEH** and **4-TPEH** showed a bathochromic shift for the major bands with the absorption extending to > 400 nm, clearly reflecting a strong π-conjugation between helicene and TPE through the alkynyl bridge. The ECD curves of *P*- and *M*-**2-TPEH** revealed a series of Cotton effects which were significantly shifted into the longer wavelength region compared to that of the pristine [6]helicene (see Supplementary Figs. 56 and 57 for comparison),[40] echoing the extension of π-conjugation observed in the absorption spectra.[41] In a tremendous contrast, *P*- and *M*-**4-TPEH** showed analogous Cotton effects like the pristine [6]helicene in the relatively shorter wavelength region even though the absorption curve were apparently bathochromically shifted.

Both **2-TPEH** and **4-TPEH** showed typical AIE feature where no obvious emission was observed

in the THF solution, but upon aggregation with the water fraction increased to 95% (see Supplementary Figs. 46 and 47 for luminescence spectra with different water fractions), strong green luminescence centered at ca. 500 nm was detected with high quantum yields of 33.9% and 37.0%, respectively (Fig. 1c left). Importantly, **2-TPEH** was CPL active with $|g_{lum}|$ = ca. 0.001 at 500 nm, while **4-TPEH** was inactive.
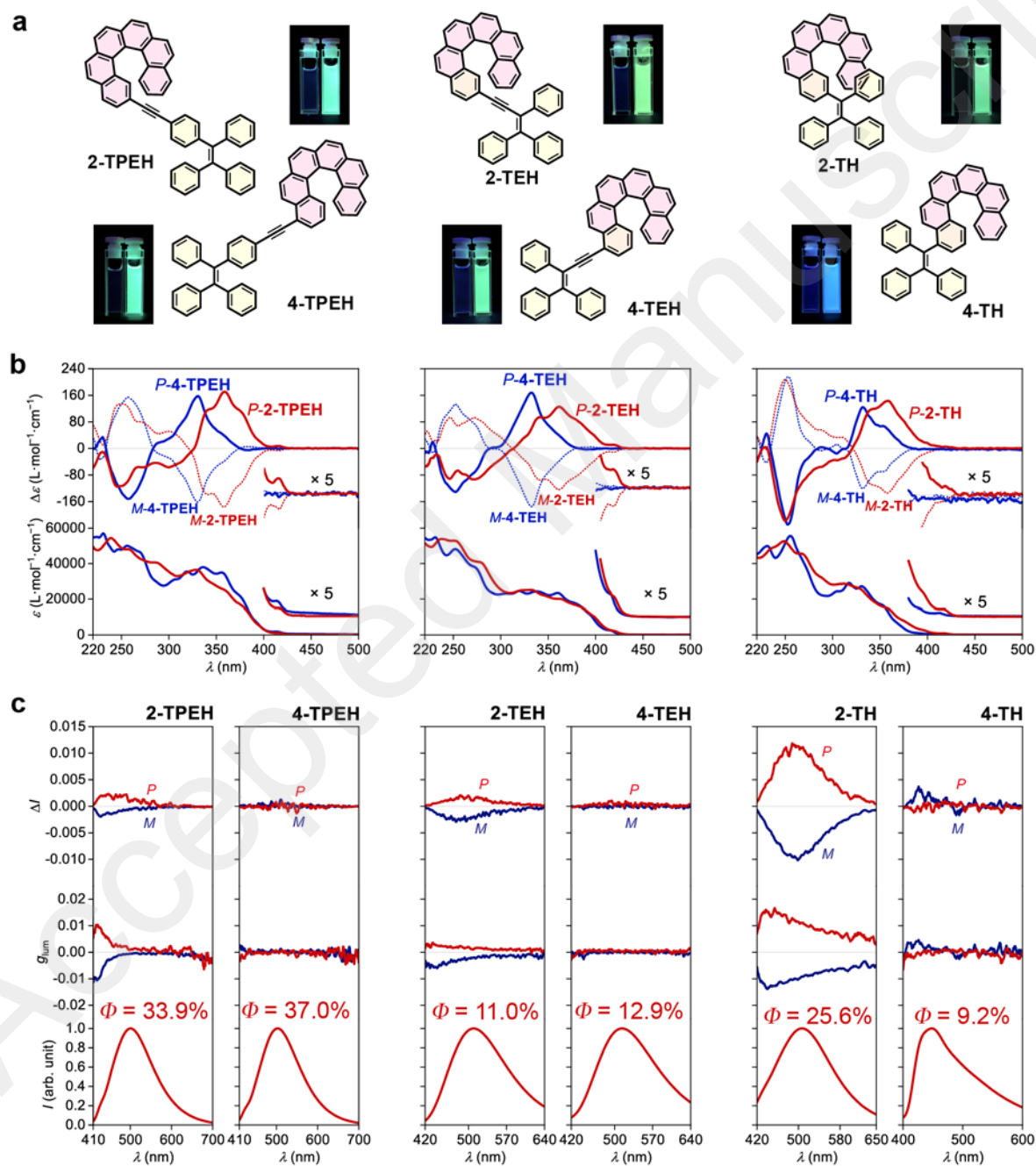

Figure 2 | Fully conjugated AIE-helicene adducts. (a) Molecular structures of **TPEH**, **TEH** and **TH** with different substitution positions (2 and 4) and corresponding photographs showing their luminescence behavior in THF (left) and a mixture of THF and H$_2$O (1 : 19, v/v) (right) with a concentration of 2.0×10^{-5} mol·L^{-1} under

365 nm UV light irradiation. (b) UV-vis and ECD spectra of **TPEH**, **TEH** and **TH** in THF with a concentration of 2.0×10^{-5} mol·L^{-1} at 298 K. (b) Luminescence, CPL and g_{lum} spectra of **TPEH**, **TEH** and **TH** in a mixture of THF and H$_2$O (1 : 19, *v/v*) with a concentration of 2.0×10^{-5} mol·L^{-1} at 298 K with excitation at 365 nm.

To decrease the distance between helicene and the AIE luminophore and hence possibly promote the chirality transfer from helicene to TPE, next, we prepare **TEH** and **TH** by removing the connective benzene ring of TPE and further the CC triple bond (Fig. 2a middle and right, see Supplementary Methods for synthetic details). **2-TEH**, **4-TEH** and **2-TH** showed stronger absorption in the visible region (> 400 nm), indicating a well-conjugated structure similar to **TPEH**. Nevertheless, **4-TH** showed no obvious absorption > 380 nm, probably because that the huge steric hindrance weakened the conjugation. As shown in Fig. 2b middle and right, similar to **2-TPEH**, **2-TEH** and **2-TH** showed relatively bathochromically shifted Cotton effects compared with the pristine carbo[6]helicene, while **4-TEH** and **4-TH** exhibit analogous CD curves like **4-TPEH** (see Supplementary Figs. 56 and 57 for comparison).

It was found that **2-TEH**, **4-TEH** and **2-TH** were typically AIE active and showed green luminescence ($\lambda_{em,max}$ = 510, 515 and 506. respectively) in the aggregated state (Fig. 2c middle and right, Supplementary Figs. 48, 49 and 52). For **2-TEH** and **4-TEH**, although the AIE luminophore only have three phenyl rings, the adducts retained the AIE feature and displayed moderated quantum yields of 11.0% and 12.9%, respectively (Fig. 2c middle). For **2-TH**, the aggregates revealed a significantly higher quantum yield (up to 25.6%) (Fig. 2c right), indicating a more confined and rigid molecular structure in the aggregated state, probably due the closer approximate of the helicene and AIE moieties. On the contrary, **4-TH** was slightly blue fluorescent in the solution and revealed an aggregation-induced emission enhancement behavior upon aggregation (Supplementary Fig. 53), where a blue emission color and a relatively low quantum yield of 9.2% were detected (Fig. 2c right). Both **2-TEH** and **2-TH** are CPL active with a |g_{lum}| value of ca. 0.002 (at $\lambda_{em,max}$ = 506 nm) and 0.011 (at $\lambda_{em,max}$ = 515 nm), respectively. Apparently, the CPL performance was improved by shortening the distance between helicene and the AIE luminophore.

Besides, for **2-TH**, the spatial regulation of the phenyl rings of the AIE moiety (into a certain chiral arrangement) by helicene through steric hindrance would be another key factor for a higher $|g_{lum}|$ value. Interestingly, the 4-substituted adducts (**4-TEH** and **4-TH**) again kept CPL silent in the whole emission region, indicating a strong effect of substitution position on the CPL performance.

Bis-substituted AIE-helicene adducts

Introduction of two luminophores at both ends of helicene has been demonstrated to be an efficient pathway to tune the chiroptical properties, majorly through exciton coupling of the pedant luminophores.[39] We then synthesized **2,15-BTEH**, **4,13-BTEH**, **2,15-BTH** and **4,13-BTH** by tethering two AIE luminophores onto a single helicene (Fig. 3a, see Supplementary Methods for synthetic details).
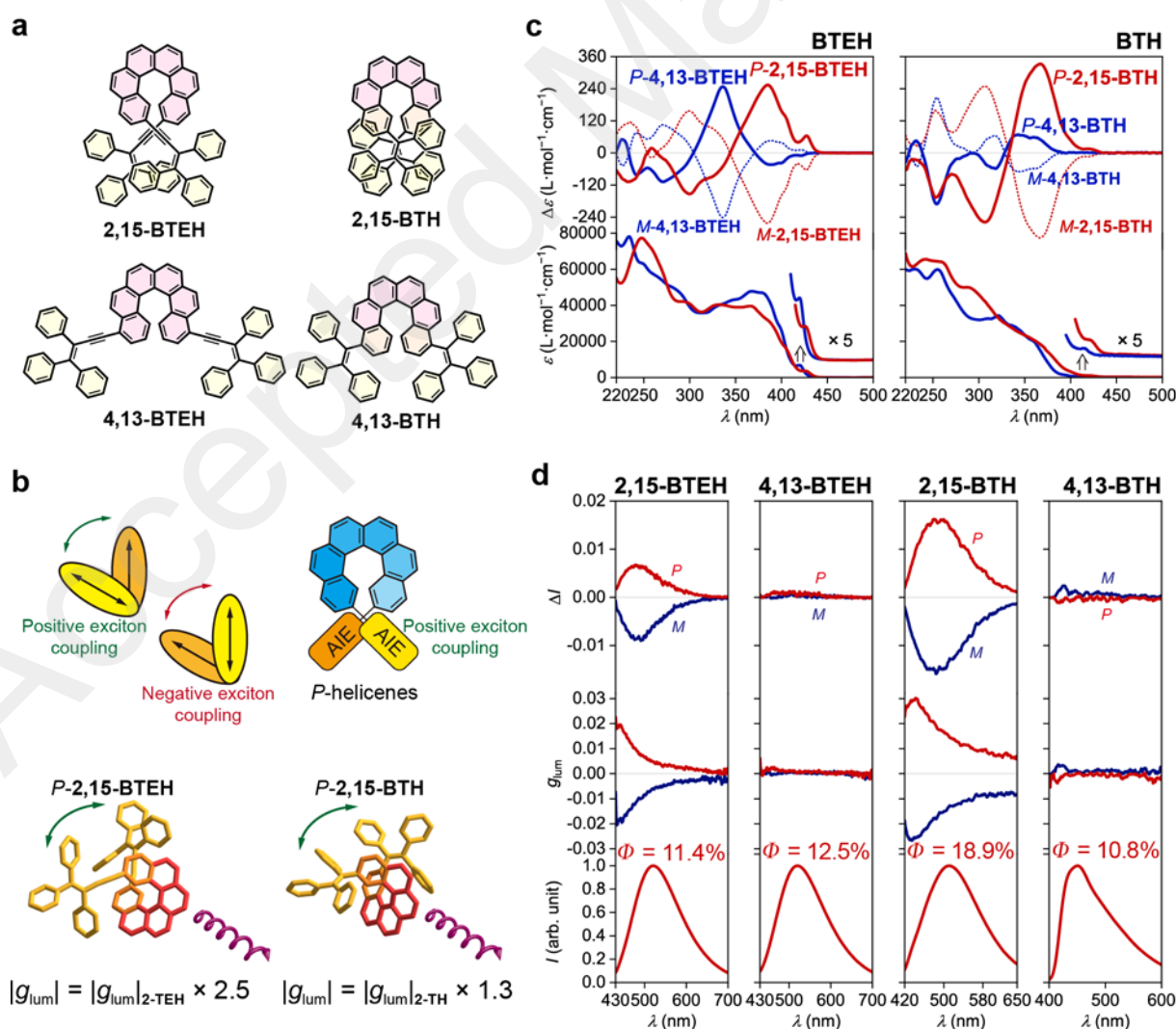
Figure 3 | Bis-substituted AIE-helicene adducts. (a) Molecular structures of **2,15-BTEH**, **4,13-BTEH**, **2,15-BTH** and **4,13-BTH**. (b) Illustrative representation of exciton couplings and crystal structures of *P*-**2,15-BTEH** and *P*-**2,15-BTH** with a positive exciton coupling and consequently, an enhanced $|g_{lum}|$ value compared to the mono-substituted **2-TEH** and **2-TH** analogues, respectively. (c) UV-vis and ECD spectra of **BTEH** and **BTH** in THF with a concentration of 2.0×10^{-5} mol·L^{-1} at 298 K. (d) Luminescence, CPL and g_{lum} spectra of **BTEH** and **BTH** in a mixture of THF and H$_2$O (1 : 19, *v/v*) with a concentration of 2.0×10^{-5} mol·L^{-1} at 298 K with excitation at 365 nm.

The absorption spectra of all four bis-substituted AIE-helicene adducts displayed a slightly bathochromic shift compared with their mono-substituted homologues and showed stronger ε values (e.g., $> 7 \times 10^5$ L·mol^{-1}·cm^{-1} at ca. 250 nm) probably due to the additional luminophores (Fig. 2c). However, the absorption bands were limited in the range of < 440 nm, without strong extension to the longer wavelength compared with their mono-substituted analogues, indicating a weak conjugation between the two luminophores through the helicene backbone. In the ECD spectra, both *P*-**2,15-BTEH** and *P*-**4,13-BTEH** showed a significantly increased Cotton effect at 385 nm ($\Delta\varepsilon = +253$ L·mol^{-1}·cm^{-1}) and 336 nm ($\Delta\varepsilon = +247$ L·mol^{-1}·cm^{-1}), respectively. Interestingly, for *P*-**2,15-BTH**, the intensity ($\Delta\varepsilon = +332$ L·mol^{-1}·cm^{-1}) of the Cotton effect at 366 nm also doubled compared to the mono-substituted **2-TH**. However, for *P*-**4,13-BTH**, the intensity of the Cotton effect at 340 nm was diminished to $+68$ L·mol^{-1}·cm^{-1}, just half of that shown by **4-TH**.

The emission of these bis-substituted AIE-helicene adducts inherited the feature of their mono-substituted analogues. For example, **2,15-BTEH**, **4,13-BTEH** and **2,15-BTH** displayed typical AIE feature with a green emission color with $\lambda_{em,max}$ = ca. 510 to 520 nm, and **4,13-BTH** showed a blue emission with a relatively low quantum yield (10.8%). Both **2,15-BTEH** and **2,15-BTH** were CPL active and showed a significantly increased $|g_{lum}|$ value of ca. 0.005 (at $\lambda_{em,max}$ = 520 nm, ca 2.5 folders of **2-TEH**) and 0.015 (at $\lambda_{em,max}$ = 510 nm, ca 1.3 folders of **2-TH**), respectively (Fig. 4d). However, for **4,13-BTEH** and **4,13-BTH**, no obvious CPL signal was detected.

Discussion and conclusion

Generally, g_{lum}, emitting color and quantum yield can be recognized as the three key factors for the evaluation of CPL materials (Fig. 1d). Amongst, emitting color and quantum yield weigh the luminescence property and are universal for all luminescent materials. However, g_{lum} is specifically associated with chiral luminescent materials, which reflects the ability of emitting circularly polarized lights. In this work, we were able to modulate these three factors by tuning of the linkage between helicene and the AIE luminophores (Fig. 4).
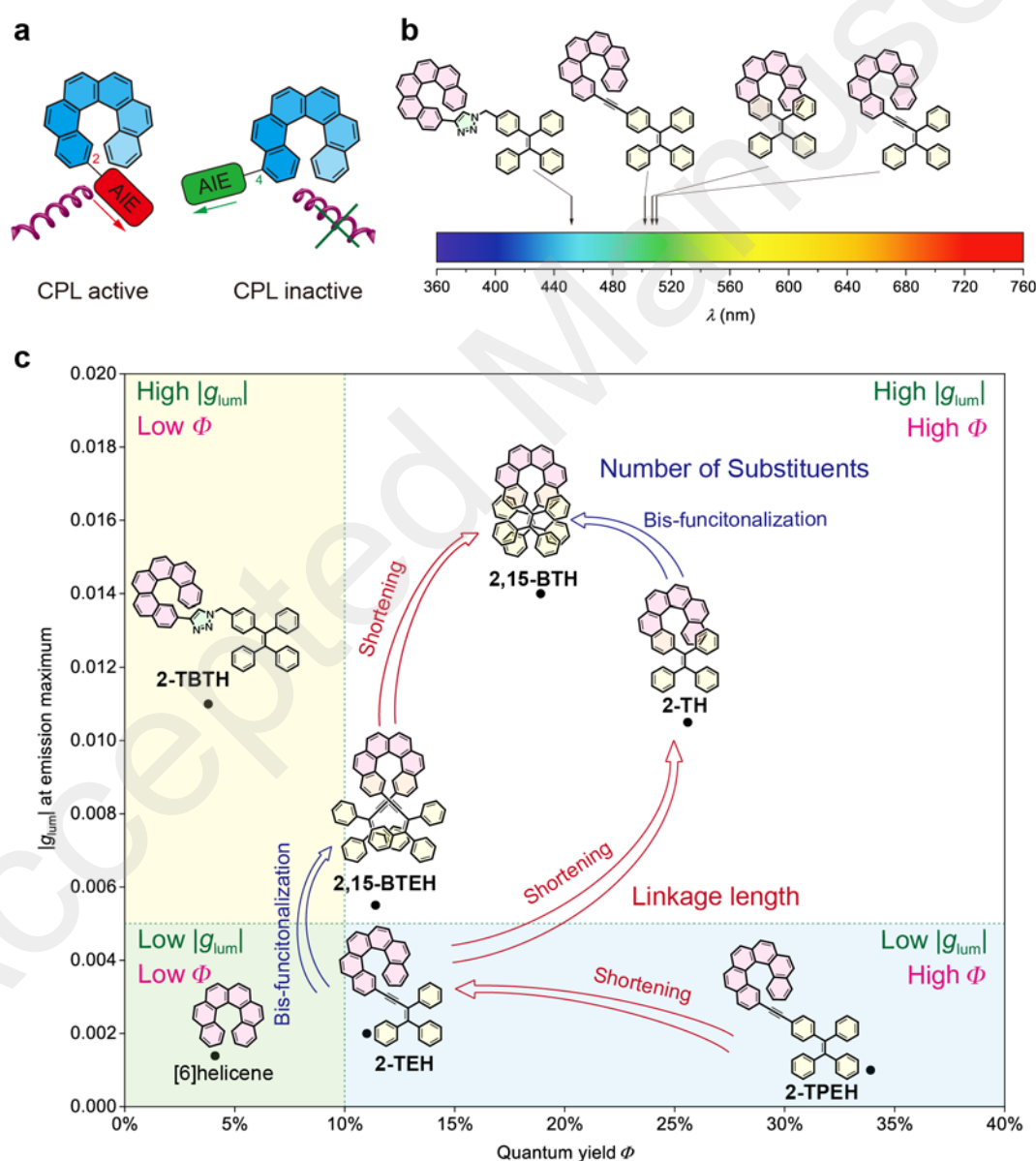

Figure 4 | Rules for CPL performance of AIE-helicene adducts. (a) Effect of linkage position on CPL capability. (b and c) Effect of linkage conjugation and length, and number of substituents on (b) emission color

and (c) $|g_{lum}|$ and quantum yield Φ.

The linkage position shows dominating influence on the CPL signals (Fig. 4a). In this work, all the 2- (or 2,15-) substituted AIE-helicene adducts appear to be CPL active while all the 4- (or 4,13-) substituted analogues are CPL inactive. This probably can be interpreted by the cancellation of contributions from various rotational conformers (rotamers) (Fig. 5). For **2-TEH** and **2-TH**, we found that the four most reasonable rotamers all provide positive ECD signals in the region > 380 nm for the P enantiomers. On the contrary, the ECD signal of **4-TEH** or **4-TH** in the larger wavelength region varies with different conformations, and the averaged ECD spectra show a serious cancellation. The CPL performance (emission corresponding to the S_1 to S_0 transition) of these molecules is strongly associated to the ECD in the lower energy band (absorption corresponding to the S_0 to S_1 transition).[19] Consequently, the 2-substituted adducts are CPL active, while the 4-substituted analogues appear to be CPL silent. It should be noted that the linkage position also shows an obvious influence on the emitting color and quantum yield for the **TH** and **BTH** derivatives.

On the other hand, the linkage conjugation majorly tunes the emitting color. For **TBTH**, due to the break of conjugation, the emitting color is limited in the blue region. On the contrary, the full conjugation of the helicene and AIE luminophore moieties in **TPEH**, **TEH** and **TH** reduces the energy gap of the electronic transitions, rendering the emission bands both shift to the longer wavelength region (Fig 4b). Besides, the conjugated linkages generally guarantee the AIE performance and a relatively high quantum yield in the aggregated state.

Compared to other variations, the linkage length predominantly modulates g_{lum}. With a decrease in the linkage length, the $|g_{lum}|$ value increases from 0.001 for **2-TPEH** to 0.002 for **2-TEH** and to 0.011 for **2-TH**. It is postulated that the shorter linkage facilitates the chirality transfer from helicene to the whole molecular skeleton and also reinforces the chirality regulation of the conformation of the AIE luminophore by the helicene moiety via steric hindrance. This is indicated by the DFT calculation on the occupancy of various rotamers for **2-TEH** and **2-TH** (compare Figs.

5a and 5c). Moreover, the shorter linkage also promotes the orbital association of helicene and the AIE luminophore, which would be helpful for a higher $|g_{lum}|$ value. Notably, the number of linkages is another important factor for g_{lum} modulation.
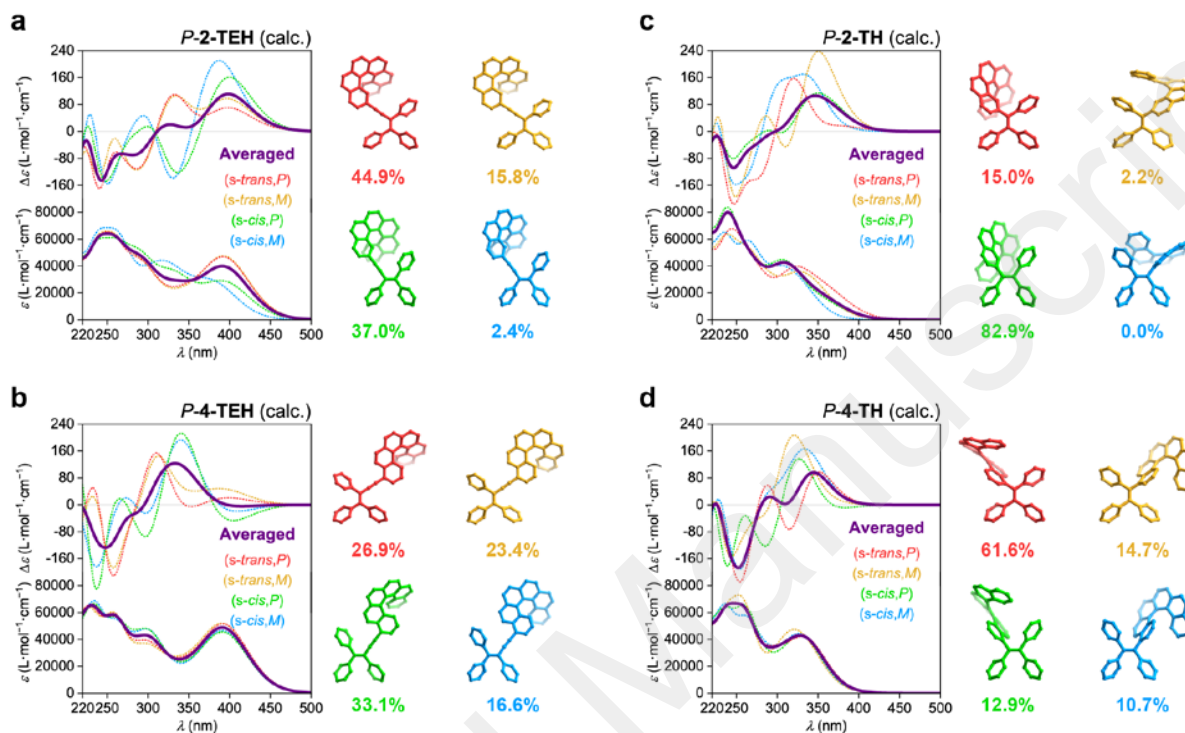

Figure 5 | Theoretical calculation results of TEH and TH. DFT-optimized structures of four most reasonable rotamers with a relative occupancy estimated from Boltzmann distribution at 298.15 K for (a) *P*-**2-TEH**, (b) *P*-**4-THE**, (c) *P*-**2-TH** and (d) *P*-**4-TH**, and their calculated absorption and ECD spectra (dash lines) and the averaged absorption and ECD spectra (purple solid lines). DFT and TD-DFT calculations were performed at B3LYP/6-311G(d,p) level with SMD continuum solvent model for THF, and the spectra were simulated following a Gaussian function centered at vertical excitation energies with a half-width at half height of 0.25 eV and were shifted by +0.2 eV for better matching. The averaged spectra were weighted by the relative occupancy.

In summary, we have demonstrated a facile pathway to prepare CPL-active AIE materials by flexible tethering of helicene and AIE luminophores. The resulting adducts showed tunable emission colors from blue to green, high luminescence intensity (quantum yield up to 37%), and large $|g_{lum}|$ values up to 0.015 in the aggregated state. These AIE-helicene adducts are expected to be employed for further applications in, for example, organic light-emitting diodes with circularly

polarized light emission and anti-fake polarized inks. Besides, the synthetic methods and structure-performance rules developed in this work would also be useful for the construction of advanced CPL materials.

Methods

Synthetic procedures and characterizations. All the synthetic experiments were performed using standard Schlenk techniques. Starting materials and reagents were of AR grade quality, which were purchased from commercial sources and used without further purification unless otherwise noted. Detailed synthetic procedures were reported in Supplementary Methods. NMR spectra were recorded on a Bruker Avance III HD 500 spectrometer or a Bruker Avance III HD 400 spectrometer. ^{1}H NMR and ^{13}C NMR analyses were also performed in Supplementary Methods, and their spectra were provided in Supplementary Figs. 1–32. Chemical shifts were determined using residual signals of the deuterated solvents or using TMS as the internal standard and were reported in parts per million (ppm). Due to the rotational barrier from excessive steric hindrance, **4-TH** and **4,13-BTH** showed multiple rotamers in ^{1}H NMR, and by variable temperature NMR, partial merging of the rotamer peaks were observed up to 373 K (Supplementary Figs. 29 and 32). MS spectra of **4-TH** and **4,13-BTH** were recorded on a Bruker SolariX 7.0 T Fourier Transform Ion Cyclotron. Single crystals of *rac*-2,15- bis(pinacolatoboryl)[6]helicene, *rac*-**2-TEH**, *rac*-**4-TEH**, *P*-**2,15-BTEH**, *M*-**4,13-BTEH**, *rac*-**2-TH**, *rac*-**4-TH**, *rac*-**2,15-BTH** and *P*-**2-TH** were obtained by slow evaporation method (details see Supplementary Methods), and their data were collected on a Bruker SMART APEX II CCD-based X-ray diffractometer with graphite-monochromatic Cu-Kα radiation ($\lambda = 1.54178$ Å) or Mo-Kα radiation ($\lambda = 0.71073$ Å) (See Supplementary Tables 1–3 for the crystal data and structure refinement, and Supplementary Figs. 35–43 for the structures). UV-vis spectra were recorded using a Lambda 35 UV-vis spectrometer, and ECD spectra were recorded on a JASCO T-815 spectropolarimeter at 293 K in a 1 cm quartz cell. The emission spectra were recorded on a Horiba Fluorolog-3 spectrometer or on a Perkin Elmer LS 55 Luminescence

Spectrometer, and the CPL spectra were recorded on a JASCO CPL-300 Spectrophotometer. The emission spectra of all the AIE-helicene conjugates with variation of water fraction were presented in Supplementary Figs. 44–55.

Theoretical calculations. For clarity and simplicity, we adopted the *P*-enantiomers for the calculations. Due to the rotations of single bonds on the molecules, *P*-**2-TH** and *P*-**4-TH** contains four reasonable rotamers, namely, (s-*trans*,*P*), (s-*trans*,*M*), (s-*cis*,*P*) and (s-*cis*,*M*) where s-*trans*/s-*cis* for the stereochemistry of the single bond between helicene and C=C bond of TPE core, while *M*/*P* for the chirality of the TPE unit. Similarly, *P*-**2,15-BTH** and *P*-**4,13-BTH** has 10 reasonable rotamers with part of them possessing the degeneracy number of 2. DFT calculations were performed using Gaussian 09 program.[42] All geometries were optimized at B3LYP/6-311G(d,p) level[43] with SMD continuum solvent model for THF[44] without any symmetry assumptions. Harmonic vibration frequency calculations were performed at the same level for verifying the resulting geometries as local minima (with zero imaginary frequency). Occupancy for each conformation was calculated according to the Gibbs free energy of each conformer following a Boltzmann distribution at 298.15 K according to Eq. 1 for *P*-**2-TH** and *P*-**4-TH**, and Eq. 2 for *P*-**2,15-BTH** and *P*-**4,13-BTH**.

$$p_i = \frac{n_i}{\sum_j n_j} = \frac{e^{-\frac{\Delta G_i}{RT}}}{\sum_j e^{-\frac{\Delta G_j}{RT}}}, (1)$$

$$p_i = \frac{g_i n_i}{\sum_j g_j n_j} = \frac{g_i e^{-\frac{\Delta G_i}{RT}}}{\sum_j g_j e^{-\frac{\Delta G_j}{RT}}}, (2)$$

Where the *p* is the occupancy for the conformation, ΔG is the relative Gibbs free energy according to the conformation with lowest energy, *R* is the gas constant, *T* is the temperature in Kelvin and *g* is degeneracy of the rotamers. The results of energy calculations were presented in Supplementary Tables 4–11. TD-DFT calculations for each conformer were also performed at B3LYP/6-311G(d,p) level with SMD continuum solvent model for THF using optimized structures by Gaussian 09

program. The simulated UV-vis and ECD spectra of **BTEH** and **BTH** were presented in Supplementary Figs. 64–71.

Data availability. The authors declare that all the data supporting the findings of this study are available within the article and Supplementary Information files, and also are available from the authors upon reasonable request.

References

1. Berova, N., Polavarapu, P. L. Nakanishi, K. & Woody, R. W. *Comprehensive chiroptical spectroscopy: Instrumentation, methodologies, and theoretical simulations* Vol. 1 (John Wiley & Sons, Inc. Hoboken, 2012).

2. Sharma, V., Crne, M., Park, J. O. & Srinivasarao, M. Structural Origin of circularly polarized iridescence in jeweled beetles. *Science* **325,** 449–451 (2009).

3. Chiou, T.-H. *et al.* Circular polarization vision in a stomatopod crustacean. *Curr. Biol.* **18,** 429–434 (2008).

4. Gagnon, Y. L., Templin, R. M., How, M. J. & Marshall, N. J. Circularly polarized light as a communication signal in mantis shrimps *Curr. Biol.* **25,** 3074–3078 (2015).

5 Sherson, J. F. *et al.* Quantum teleportation between light and matter. *Nature* **443,** 557–560 (2006).

6. Wang, C., Fei, H., Qiu, Y., Yang, Y. & Wei, Z. Photoinduced birefringence and reversible optical storage in liquid-crystalline azobenzene side-chain polymers. *App. Phys. Lett.* **74,** 19–21 (1998).

7. Zheng, H. *et al.* Uncovering the circular polarization potential of chiral photonic cellulose films for photonic applications. *Adv. Mater.* **30,** 1705948 (2018).

8. Seitz, M., Moore, E. G., Ingram, A. J., Muller, G. & Raymond, K. N. Enantiopure, octadentate ligands as sensitizers for europium and terbium circularly polarized luminescence in aqueous solution. *J. Am. Chem. Soc.* **129,** 15468–15470 (2007).

9. Yuasa, J. *et al.* Fingerprint signatures of lanthanide circularly polarized luminescence from proteins covalently labeled with a β-diketonate europium(III) chelate. *Chem. Commum.* **49,** 4604–4606 (2013).

10. Song, F. *et al.* Chiral sensing for induced circularly polarized luminescence using an Eu(III)-containing polymer and D- or L-proline. *Chem. Commum.* **49,** 5772–5774 (2013).

11. Shuvaev, S., Suturina, E. A., Mason, K. & Parker, D. Chiral probes for α_1-AGP reporting by species-specific induced circularly polarised luminescence. *Chem. Sci.* **9,** 2996–3003 (2018).

12. Sato, I., Sugie, R., Matsueda, Y., Furumura, Y. & Soai, K. Asymmetric synthesis utilizing circularly polarized light mediated by the photoequilibrium of chiral olefins in conjunction with asymmetric autocatalysis. *Angew. Chem. Int. Ed.* **43,** 4490–4492 (2004).

13. Richardson, R. D. *et al.* Dual wavelength asymmetric photochemical synthesis with circularly polarized light. *Chem. Sci.* **6,** 3853–3862 (2015).

14. Yang, Y., da Costa, R. C., Fuchter, M. J. & Campbell, A. J. Circularly polarized light detection by a chiral organic semiconductor transistor. *Nat. Photonics* **7,** 634–638 (2013).

15. Yang, Y., Da Costa, R. C., Smilgies, D.-M., Campbell, A. J. & Fuchter, M. J. Induction of circularly polarized electroluminescence from an achiral light-emitting polymer via a chiral small-molecule dopant. *Adv. Mater.* **25,** 2624–2628 (2013).

16. Brandt, J. R., Wang, X., Yang, Y., Campbell, A. J. & Fuchter, M. J. Circularly polarized phosphorescent electroluminescence with a high dissymmetry factor from PHOLEDs based on a platinahelicene. *J. Am. Chem. Soc.* **138,** 9743–9746 (2016).

17. Riehl, J. P. & Richardson, F. S. Circularly polarized luminescence spectroscopy. *Chem. Rev.* **86,** 1–16 (1986).

18. Sánchez-Carnerero E. M. *et al.* Circularly polarized luminescence from simple organic molecules. *Chem. Eur. J.* **21,** 13488–13500 (2015).

19. Tanaka, H., Inoue, Y. & Mori, T. Circularly polarized luminescence and circular dichroisms in small organic molecules: correlation between excitation and emission dissymmetry factors.

ChemPhotoChem **2,** 386–402 (2018).

20. Chen, N. & Yan, B. Recent Theoretical and experimental progress in circularly polarized luminescence of small organic molecules. *Molecules* **23,** 3376 (2018).

21. Zinna, F. & di Bari, L. Lanthanide circularly polarized luminescence: bases and applications *Chirality* **27,** 1–13 (2015).

22. Kumar, J., Nakashima, T. & Kawai, T. Circularly polarized luminescence in chiral molecules and supramolecular assemblies *J. Phys. Chem. Lett.* **6,** 3445–3452 (2015).

23. Roose, J., Tang, B. Z. & Wong, K. S. Circularly-polarized luminescence (CPL) from chiral AIE molecules and macrostructures. *Small* **12,** 6495–6512 (2016).

24. Hong, Y., Lam, J. W. Y. & Tang, B. Z. Aggregation-induced emission. *Chem. Soc. Rev.* **40,** 5361–5388 (2011).

25. Mei, J., Leung, N. L. C., Kwok, R. T. K. Lam, J. W. Y. & Tang, B. Z. Aggregation-induced emission: together we shine, united we soar! *Chem. Rev.* **115,** 11718–11940 (2015).

26. Zhang, S. *et al.* Circularly polarized luminescence of AIE-active chiral O-BODIPYs induced via intramolecular energy transfer. *Chem. Commun.* **51,** 9014–9017 (2015).

27. Sheng, Y. et al. Reversal circularly polarized luminescence of AIE-active chiral binaphthyl molecules from solution to aggregation. *Chem. Eur. J.* **21,** 13196–13200 (2015).

28. Shen, Y. & Chen, C.-F. Helicene: synthesis and application. *Chem. Rev.* **112,** 1463–1535 (2012).

29. Gingras, M. One hundred years of helicene chemistry. Part 1: non-stereoselective syntheses of carbohelicenes. *Chem. Soc. Rev.* **42,** 968–1006 (2013).

30. Nakamura, K., Furumi, S., Takeuchi, M., Shibuya, T. & Tanaka, K. Enantioselective synthesis and enhanced circularly polarized luminescence of S-shaped double azahelicenes. *J. Am. Chem. Soc.* **136,** 5555–5558 (2014).

31. Murayama, K. *et al.* Enantioselective synthesis, crystal structure, and photophysical properties of a 1,1′-bitriphenylene-based sila[7]helicene. *Eur. J. Org. Chem.* **2015,** 1409–1414 (2015).

32. Kaseyama, T., Furumi, S., Zhang, X., Tanaka, K. & Takeuchi, M. Hierarchical assembly of a phthalhydrazide-functionalized helicene. *Angew. Chem. Int. Ed.* **50,** 3684–3687 (2011).

33. Oyama, H. *et al.* Synthesis and properties of [7]helicene-like compounds fused with a fluorene unit. *Org. Lett.* **18,** 3654–3657 (2016).

34. Shen, C. *et al.* Straightforward access to mono- and bis-cycloplatinated helicenes displaying circularly polarized phosphorescence by using crystallization resolution methods. *Chem. Sci.* **5,** 1915–1927 (2014).

35. Cruz, C. M. *et al.* Undecabenzo[7]superhelicene: a helical nanographene ribbon as a circularly polarized luminescence emitter. *Angew. Chem. Int. Ed.* **57,** 14782–14786 (2018).

36. Leung, N. L. C. *et al.* Restriction of intramolecular motions: the general mechanism behind aggregation-induced emission. *Chem. Eur. J.* **20,** 15349–14353 (2014).

37. Zhao, Z. *et al.* Steric hindrance, electronic communication, and energy transfer in the photo- and electroluminescence processes of aggregation-induced emission luminogens. *J. Phys. Chem. C* **114,** 7963–7972(2010).

38. Schaack, C. *et al.* Helicene monomers and dimers: chiral chromophores featuring strong circularly polarized luminescence. *Chem. Eur. J.* **25,** 8003–8007(2019).

39. Dhbaibi, K. *et al.* Exciton coupling in diketopyrrolopyrrole–helicene derivatives leads to red and near-infrared circularly polarized luminescence. *Chem. Sci.* **9,** 735–742 (2018).

40. Nakai, Y., Mori, T. & Inoue, Y. Theoretical and experimental studies on circular dichroism of carbo[*n*]helicenes. *J. Phys. Chem. A* **116,** 7372–7385 (2012).

41. Moussa, M. E. S. et al. Chiroptical properties of carbo[6]helicene derivatives bearing extended π–conjugated cyano substituents. *Chirality* **25,** 455–465(2013).

42. Frisch, M. J. *et al. Gaussian 09, Revision E.01* (Gaussian, Inc., 2009).

43. Lee, C., Yang, W. & Parr, R. G. Development of the Colle-Salvetti correlation-energy formula into a functional of the electron density. *Phys. Rev. B: Condens. Matter Mater. Phys.* **37,** 785–789 (1988).

44. Marenich, A. V., Cramer, C. J. & Truhlar, D. G. Universal solvation model based on solute electron density and on a continuum model of the solvent defined by the bulk dielectric constant and atomic surface tensions. *J. Phys. Chem. B* **113,** 6378–6396 (2009).

Acknowledgements

Author contributions

C.S. and H.Q. conceived the project. C.S., F.G., G.Z., Y.D. and J.W. synthesized all the compounds. C.S., F.G., G.Z., Y.D. and J.W. conducted the spectroscopic experiments and data analysis with R.W.' assistance. C.S. conducted the theoretical calculation. C.S. and H.Q. wrote the manuscript with inputs from J.C. All authors discussed the results and commented on the manuscript.

Additional information

Supplementary Information accompanies this paper at http://www.nature.com/ naturecommunications

Competing interests: The authors declare no competing financial interests.